

Unsupervised Time-series Fatigue Damage State Estimation of Complex Structure Using Ultrasound Based Narrowband and Broadband Active Sensing

S.Mohanty¹, A. Chattopadhyay², J. Wei³ and P. Peralta⁴

Abstract: This paper proposes unsupervised system identification based methods to estimate time-series fatigue damage states in real-time. Ultrasound broadband input is used for active damage interrogation. Novel damage index estimation techniques based on dual sensor signals are proposed. The dual sensor configuration is used to remove electrical noise, as well as to improve spatial resolution in damage state estimation. The scalar damage index at any particular damage condition is evaluated using nonparametric system identification techniques, which includes an empirical transfer function estimation approach and a correlation analysis approach. In addition, the effectiveness of two sensor configurations (configuration 1: sensors placed near the actuator and configuration 2: sensors placed away from the actuator) are evaluated. Furthermore, the time series 2σ error bound is also evaluated to study the effect of measurement noise on damage state estimation. The time-series damage estimation approaches are validated on a complex A1-2024 cruciform specimen undergoing biaxial cyclic loading.

Keywords: Structural Health Monitoring (SHM), on-line state estimation, damage index, nonparametric system identification, frequency response analysis, correlation analysis, active sensing, ultrasound broadband input

1 Introduction

Real-time health monitoring and prognostics are emerging at the forefront of Condition Based Maintenance (CBM) of critical structural systems. Whether it is a newly acquired or an aging aircraft fleet, the structural life ceiling of the fleet is defined from three distinct approaches: safe-life, fail-safe, and damage tolerant ap-

¹ Graduate Student, Mechanical and Aerospace Engineering, ASU, Tempe, AZ, USA.

² Fellow ASME, AIAA, Professor, Mechanical and Aerospace Engineering, ASU, Tempe, AZ, USA.

³ Assistant Professor Research, Mechanical and Aerospace Engineering, ASU, Tempe, AZ, USA.

⁴ Associate Professor, Mechanical and Aerospace Engineering, ASU, Tempe, AZ, USA.

proaches. A detailed review of these approaches is presented by Iyyer, Sarkar, Merrill, and Phan (2007). In the above mentioned approaches the damage tolerance and fatigue life predictions are obtained based on assumed structural flaws or on previous coupon test results, regardless of whether the assumed structural flaws actually occur in service. Consequently, a large degree of conservatism is incorporated into structural designs due to these uncertainties. The current state of the art in the area of on-line (Farrar, Sohn, and et. al. (2003), Farrar, Worden, and et. al. (2007), Mohanty, Chattopadhyay, Wei, and Peralta (2009), Mohanty, Chattopadhyay, and Peralta (2009)) damage state estimation, or structural health monitoring (SHM) techniques, offers methodologies for adaptive damage state prediction and residual useful life assessment. At present, both passive vibration based global damage detection approaches and active Lamb wave based local damage detection approaches are widely being studied by the SHM research community. The Lamb wave method using a pitch-catch approach (Giurgiutiu and Cuc (2005)) has been used to identify the changes in the transmission velocity or energy of the elastic waves associated with damage. Different pattern recognition techniques, (Park, Yun, Roh, and Lee (2006)) such as support vector machine for damage classification are used to correlate the Lamb wave active signal to find a practical damage indicator. However, it is noted that most of the pattern recognition algorithms require large training data sets to extrapolate physically meaningful information for an unknown damage condition. To circumvent this problem the use of system identification (Ljung (1999), Klein and Morelli (2006)) techniques for damage state identification can be explored. However, many of the available approaches on system identification are generally confined to low frequency applications such as process and aircraft flight control identification. The research on low frequency structural damage identification, such as vibration based damage identification (Giurgiutiu and Cuc (2008)) has limitations because of the large power and actuator requirements to excite the low frequency, global structural modes. However, for local damage identification, smaller piezoelectric based actuators with low power requirements can be used to generate the required deterministic input signals for effective use of system identification tools. The use of fairly matured system identification techniques can be extended for high frequency Lamb wave input signals in the range of kHz to MHz. For example, the high frequency response function (Park, Rutherford, and et. al. (2005)) can be estimated at a particular damage condition and can be compared with the frequency response function of the other damage condition to evaluate the relative change in the structural health. It is noted that the narrowband Lamb wave input widely used in the SHM community has limited capability for persistence of excitation except around the central frequency of the chosen input signal. Input signals such as multisine (Rivera, Lee, Mittelman, and Barun (2007)) signals can be used for persistence excitation in a broader frequency band of interest. Under

experimental conditions where environmental noise is persistent, multiple cycles of the periodic input can be introduced until the variance in the model estimate is reduced to acceptable levels. In the present paper, both narrowband and broadband chirp (Xiang-Gen (1997)) input is used to estimate the time series damage states. It is noted that the chirp signal used in the present case is a type of multisine signal. However, the individual harmonics are not optimized but rather linearly varied harmonics are selected in the required broadband frequency domain for simplicity. Additionally, the paper presents the use of two nonparametric system identification approaches such as frequency-domain based empirical transfer function estimation approach and time-domain based correlation analysis approach to estimate time series damage states. The individual damage state at a given fatigue cycle is evaluated using dual sensor approach. The detail procedure of time-series damage state estimation and its validation are discussed in the following sections.

2 Theoretical Approach

Real-time damage state estimation is an integral part of SHM and prognosis systems. For this purpose, the condition of the structure has to be assessed at real time using sensor signals acquired either continuously or discretely. As mentioned earlier, nonparametric system identification approaches based on ultrasonic deterministic input signals are explored to estimate the current state of a structure. In the present paper the effectiveness of both narrow and broadband input signal is studied. It is noted that for low frequency identification applications, where the additive noise is independent of the deterministic input signal, the noise can be removed easily using correlation analysis. However, in the case of high frequency state identification applications usually the additive noise in the acquired signals contains the input dependent noise in addition to the input independent noise. Without knowledge of a time dependent noise transfer function, it is difficult to remove the input dependant noise from the measured outputs. To avoid this problem, two sensors are placed close together. It is expected they will receive the same input dependent and independent noise, then it can be removed by taking the difference of each sensor measurement. In addition to the noise removal, the dual sensor configuration will also help to improve the spatial resolution in damage state estimation. It is noted that if two sensors are placed adjacent, they would receive ideally same signal at a given damage condition. However, if there is a small change in damage, this will be reflected as large differential change in sensor signals received at the adjacent sensors. As the damage grows this differential change grows with respect to the healthy of reference condition. This phenomenon of large differential signal change for small change in damage condition can be used for improving the spatial resolution in damage state estimation. The dual sensor configuration block

diagram is shown in Figure 1. In the figure, u is the deterministic narrow or broad-

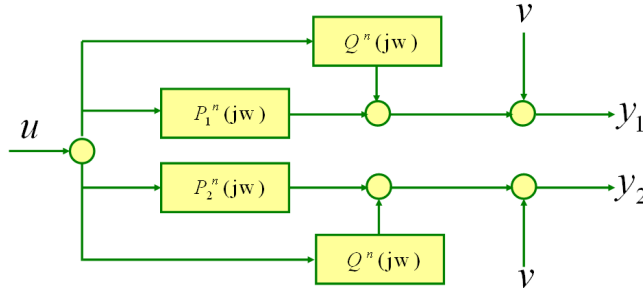


Figure 1: Input-output block diagram.

band input signal, P_1^n is the n^{th} damage level transfer function associated with input u and output y_1 from sensor 1. Similarly P_2^n is the n^{th} damage level transfer function for sensor 2. It is noted that even though the two sensors are identical and placed nearby, the transfer function associated with sensor 1 will be different compared to the transfer function associated with sensor 2. This difference is because each sensor will be receiving different reflected signals from a propagating crack or damage. However, the input dependant noise transfer function Q^n is assumed to be the same for both sensors since it is usually due to electromagnetic interference and electromagnetic compatibility. In addition, the sensor might receive input independent noise, denoted as v . With the above information, the measurement equation for both sensor 1 and 2 can be written as:

$$y_1 = P_1^n(j\omega)u + Q^n(j\omega)u + v \tag{1}$$

$$y_2 = P_2^n(j\omega)u + Q^n(j\omega)u + v \tag{2}$$

2.1 Damage state estimation using empirical transfer function estimation (ETFTE) approach

Differencing Eq. 2 from Eq. 1,

$$y_1 - y_2 = (P_1^n(j\omega) - P_2^n(j\omega))u \tag{3}$$

Eq. 3 can be equivalently written as,

$$y = P^n(j\omega)u \tag{4}$$

where $y = y_1 - y_2$ and $P^n(j\omega) = P_1^n(j\omega) - P_2^n(j\omega)$. Using spectral analysis, the transfer function $P^n(j\omega)$ can be expressed as

$$P^n(j\omega) = \frac{S_{uy}^n(j\omega)}{S_{uu}^n(j\omega)} \quad (5)$$

where $S_{uy}^n(j\omega)$ and $S_{uu}^n(j\omega)$ are the cross-spectral density between u and y , and auto-spectral density of u respectively. These densities can be expressed in terms of cross-covariance coefficients $C_{uy}(m)$ and auto-covariance coefficients $C_{uu}(m)$ as

$$S_{uy}^n(j\omega) = \sum_{k=-L}^L C_{uy}^n \omega(k) e^{-j\omega k} \quad (6)$$

$$S_{uu}^n(j\omega) = \sum_{k=-L}^L C_{uu}^n \omega(k) e^{-j\omega k} \quad (7)$$

where $\omega(k)$ is the lag window used for smoothing and L is the truncation parameter for the window. Substituting $y_1 - y_2$ for y in Eq. 6 Eq. 5 can be rewritten as

$$P^n(j\omega) = \frac{S_{uy_1}^n(j\omega) - S_{uy_2}^n(j\omega)}{S_{uu}^n(j\omega)} = P_1^n(j\omega) - P_2^n(j\omega) \quad (8)$$

where

$$P_1^n(j\omega) = \frac{S_{uy_1}^n(j\omega)}{S_{uu}^n(j\omega)}; \quad P_2^n(j\omega) = \frac{S_{uy_2}^n(j\omega)}{S_{uu}^n(j\omega)} \quad (9)$$

The frequency response function $P^n(j\omega)$ in Eq. 8 represents the change in damage condition at n^{th} damage level. It is noted that the frequency response function is a vector and to directly compare the different damage conditions using this function is difficult. An equivalent root mean square deviation (RMSD) based novel damage index a^n is proposed. The damage index is normalized against the healthy condition frequency response function and is expressed as

$$a^n = \sqrt{\frac{\sum_{\omega=\omega_f}^{\omega=\omega_i} (P^n(j\omega) - P^0(j\omega))^2}{\sum_{\omega=\omega_f}^{\omega=\omega_i} (P^0(j\omega))^2}} \quad (10)$$

where $P^n(j\omega) = P_1^n(j\omega) - P_2^n(j\omega)$. It is noted that $n = 0$ represents the reference damage level. The n^{th} level damage index a^n is the equivalent change in output (from piezoelectric sensors) time-series against a fixed input (from the piezoelectric actuator) time-series measured at the n^{th} damage level.

2.2 Damage state estimation using correlation analysis (CRA) approach

The accuracy of the damage index estimated using the ETFE approach depends on how accurately the spectral densities S_{uy} and S_{uu} are estimated. To be noted that the accurate estimation of the spectral densities depends on the accuracy in the Fourier transformation of the respective cross-covariance coefficients $C_{uy}(m)$ and auto-covariance coefficients $C_{uu}(m)$. To avoid errors in the frequency domain transformation, the time-domain cross-correlation and auto-correlation coefficients can be directly used to estimate the time-series damage indices a^n . For a deterministic, fixed input signal the auto-correlation coefficients $C_{uu}(m)$ are fixed for all damage conditions, and ignoring the contribution from the auto-correlation coefficients $C_{uu}(m)$, the equivalent damage index can be evaluated as

$$a^n = \sqrt{\frac{\sum_{m=-M}^{m=M} (R_{uy}^n(m) - R_{uy}^0(m))^2}{\sum_{m=-M}^{m=M} (R_{uy}^0(m))^2}} \quad (11)$$

where $R_{uy}^n(m) = R_{uy_1}^n(m) - R_{uy_2}^n(m)$, $R_{uy_1}^n(m)$ and $R_{uy_2}^n(m)$ are the m^{th} lagged cross-correlation coefficients corresponding to sensor 1 and sensor 2 respectively. The m^{th} lagged cross-correlation coefficients $R_{uy_i}^n(m)$ are expressed in terms of the m^{th} lagged cross-covariance function $C_{uy_i}(m)$ as

$$R_{uy_i}^n(m) = \frac{C_{uy_i}^n(m)}{\sqrt{C_{uu}^n(m)} \sqrt{C_{y_i y_i}^n(m)}} \quad (12)$$

It is noted that $n = 0$ represents the reference damage level, not necessarily the healthy or pristine condition of the structure. The damage index a^n is the representation of the n^{th} damage condition with respect to the reference ($n = 0$) or known damage condition. It is also important to mention that both the proposed damage index estimation approaches (ETFE and CRA) are valid for any complex structure and the validation of these approaches will be discussed in the following sections.

3 Fatigue Experiment and Finite Element Simulation for Data Generation

To evaluate the performance of the damage index estimation at different damage conditions, both broadband and narrowband active signals are tested. To generate the output sensor signal against the broadband actuator input, a fatigue experiment is performed, whereas for generating the output sensor signal against the narrowband actuator input, a finite element simulation is performed. It is noted that the finite element simulation is time consuming and the computational time and memory requirements increase significantly with an increase in the length of the input

signal. In this work, finite element simulations are not performed for the broadband input, rather only for the narrowband input signal.

3.1 Fatigue Experiment for Broadband Active Sensing

To test the real-time state estimation algorithm, a fatigue test was performed on an Al-2024 cruciform specimen under biaxial loads. As shown in Figure 2, the cruciform specimen was loaded using a MTS biaxial/torsion test frame. The specimen

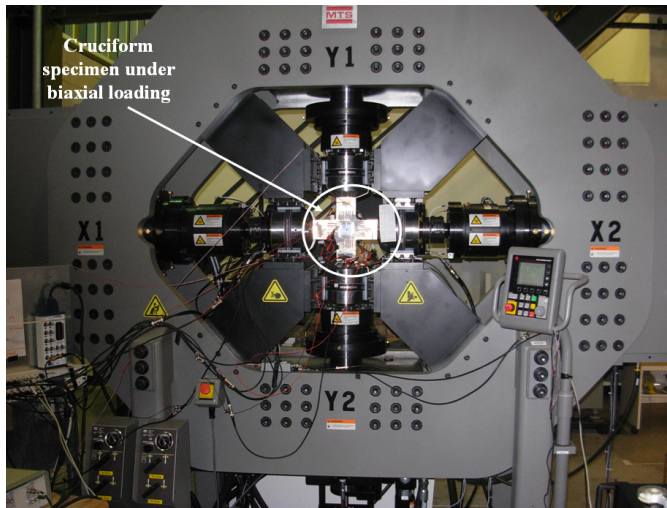


Figure 2: Experimental setup with instrumented Al-2024 cruciform specimen.

was subjected to a constant amplitude fatigue load with amplitude $\sigma_{max} = 21.36$ kN, load ratio $R=0.1$, and frequency of 10 Hz. For damage state estimation at different damage levels, piezoelectric actuators and sensors were used. The instrumented cruciform specimen with different sensor configurations can be seen in Figure 3. After each 1500 cycles, the test frame was programmed to stop for 75 seconds and during this period, piezoelectric sensor signals were collected for a deterministic (or fixed) input signal. Images of the propagating damage were also collected using a high resolution camera. The data and image collection started at approximately 10 kcycles. The image and sensor data were collected at 95 different damage levels. It should be noted that to accelerate the crack initiation process, a circular hole (refer Figure 3) was made at the center of the web area. Also, as shown in Figure 3, an EDM notch (in the bottom right quadrant of web area) of length 1 mm was made at the edge of the circular hole to further accelerate crack initiation. A through

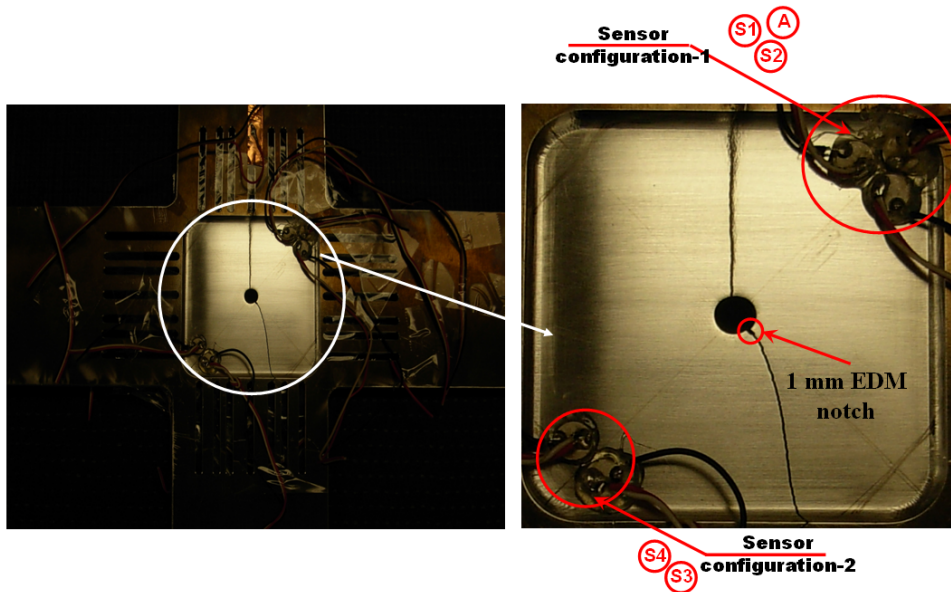


Figure 3: Cruciform specimen with different sensor configurations.

crack started from the EDM notch at approximately 19 kcycles (refer Figure 4) and grew towards the bottom edge of the web area. Once the crack reached the bottom edge of the web, a second crack initiated at the upper boundary (along the vertical axis) of the central hole. The second crack grew up to the top boundary of the web before final catastrophic failure occurred. The second crack growth was rapid and occurred only within 6 kcycles before final failure occurred at 151 kcycles. Out of the total 95 damage levels, the crack tip was in focus (of the high resolution camera) only for the first 48 images. The crack length measurement corresponding to different damage levels (or fatigue cycles) and different sequence of events can be seen in Figure 4. In the case of active sensing, the input signal considered for this study was a broadband chirp signal with frequency varying from 100 kHz to 300 kHz and is shown in Figure 5a. The persistence of excitation in the chosen band can be seen from the spectral density plot shown in Figure 5b. A representative sensor signal from sensor 1 (Ref. S1 in Figure 3) at the healthy condition is shown in Figure 5c, and the corresponding spectral density is shown in Figure 5d. From Figure 5d it can be seen that the output power spectral density, between 100 kHz to 300 kHz, is found to be persistently higher than -100dB/Hz. The persistence of excitation can also be seen from the spectrogram plots of the input and output signal shown in Figure 6a and 6b, respectively. This persistence of excitation of structural

modes in the chosen frequency band is a good indicator for unbiased state estimation. It is noted that at each damage level, 5 sets of active signals were collected

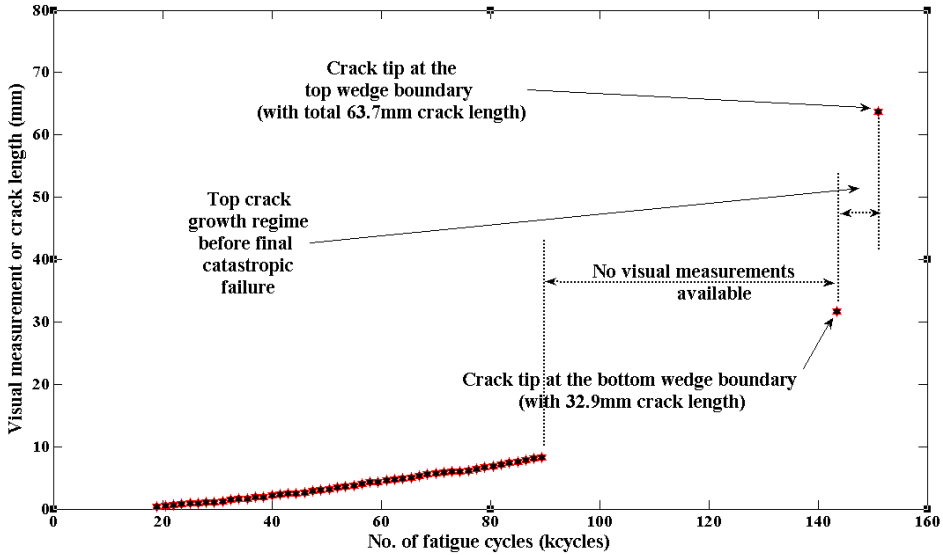


Figure 4: Visual measurements with different sequence of events.

by exciting the piezoelectric actuator in 5 seconds intervals. These multiple sets of observations at a single damage level were collected to avoid any measurement loss due to false actuation and to quantify the error bound in the damage index estimation. The measured sensor signals at different damage levels are used to estimate the corresponding damage index and will be discussed in the following section.

3.2 Finite Element Simulation for Narrowband Active Sensing

To evaluate the performance of the damage index estimation against the narrowband burst signal, finite element (FE) simulations are performed. Ten different damage cases were considered; damage case 1: healthy condition (with 1 mm notch), case 2: 5 mm bottom crack, case 3: 10 mm bottom crack, case 4: 15 mm bottom crack, case 5: 20 mm bottom crack, case 6: 25 mm bottom crack, case 7: 30 mm bottom crack, case 8: 32 mm bottom crack, case 9: 17 mm top (total crack length of 49 mm) crack, case 10: 32 mm top (total crack length of 64 mm). The finite element model for a typical case (case 10) can be seen in Figure 7a. The piezoelectric actuator and sensors are placed at the same positions as the experimental specimen shown in Figure 3. A snapshot of the wave propagation

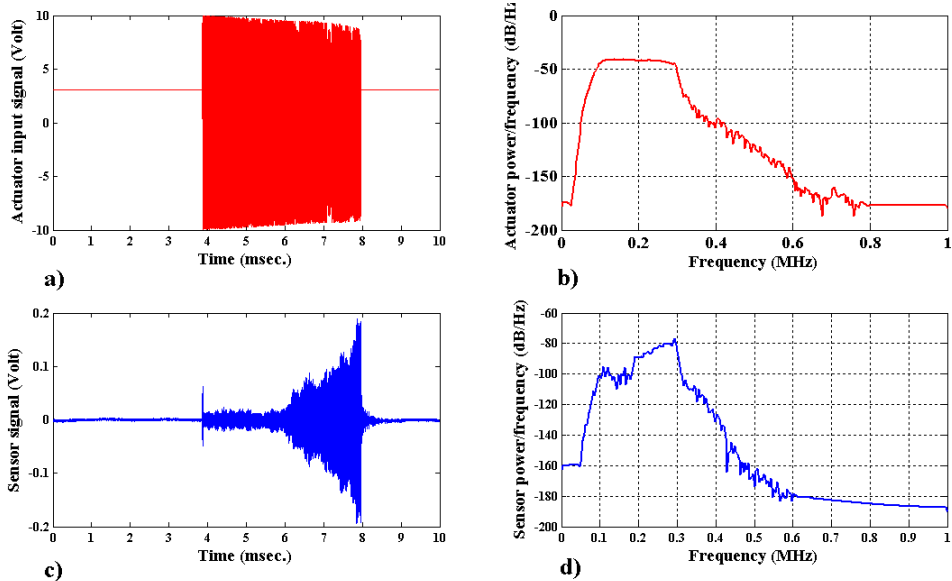


Figure 5: a) Broadband chirp input with frequency sweep from 100 kHz to 300 kHz b) Power spectral density of the input signal c) Signal from sensor 1 at a typical damage level. d) Power spectral density of the sensor signal in c).

simulation for damage case 10 can also be seen in Figure 7b. This wave propagation simulation study shows that due to the presence of a large crack in front of the actuator, sensors placed on the opposite side of the crack (e.g. sensor 3 and sensor 4 of sensor configuration 2) become blind to the traveling input waves. For all ten damage cases, the piezoelectric actuator is excited with a 230 kHz narrowband burst input as shown in Figure 8a. Figure 8b shows the power spectral density of the input signal. The sensor signal from sensor 1 and its power spectral density can be seen in Figure 8c and Figure 8d respectively. In addition, Figure 9a and 9b show the spectrograms of the actuator and sensor signals shown in Figure 8. The simulated sensor signals at different damage levels are used to estimate the damage index, which will be discussed in the following sections.

4 Numerical Results for Time Series Damage State Estimation

Sensor signals generated using the fatigue experiment and FE simulation are used for estimating the time-series damage index. The details of the results are explained in the following subsections.

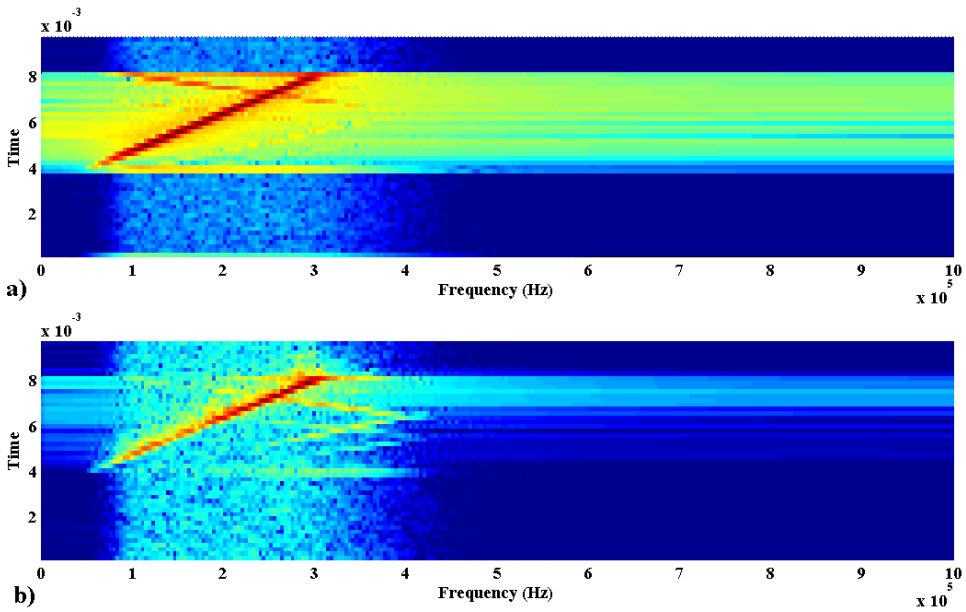


Figure 6: a) Spectrogram of input signal shown in Figure 5a and b) Spectrogram of output signal shown in Figure 5c.

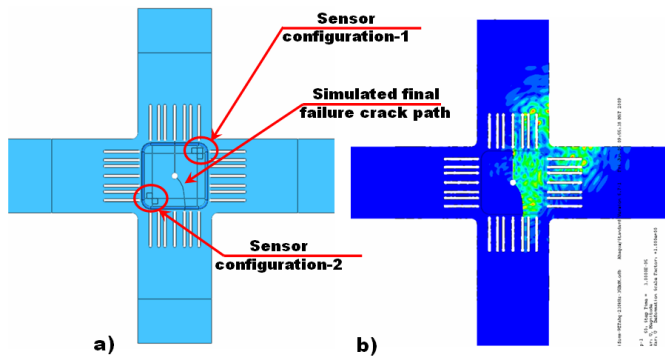


Figure 7: a) Finite element simulation showing crack path during final catastrophic failure b) Snap shot of wave propagation with simulated crack path as shown in Figure a.

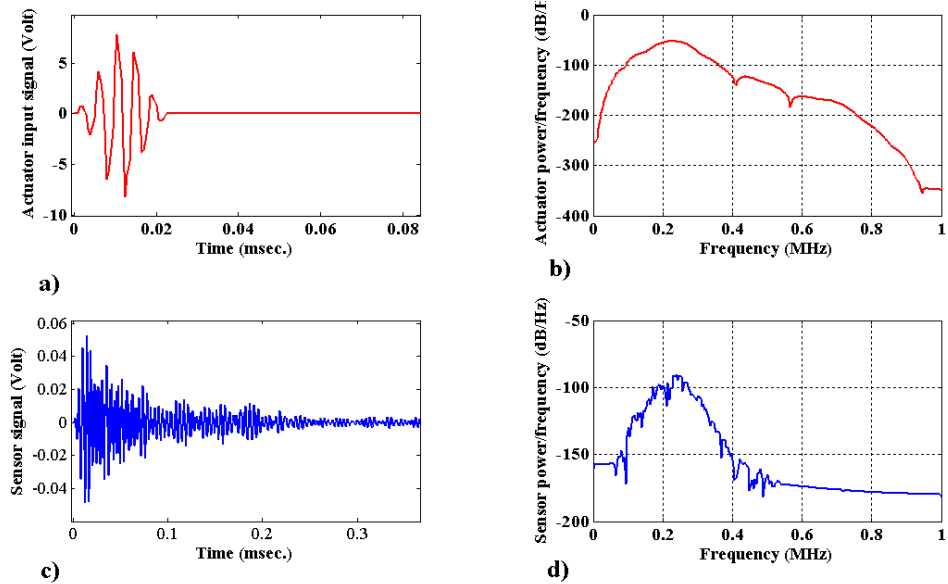


Figure 8: a) Narrowband burst input with central frequency 230 kHz b) Power spectral density of the input signal c) Sensor signal from sensor 1 d) Power spectral density of the sensor signal in Figure c.

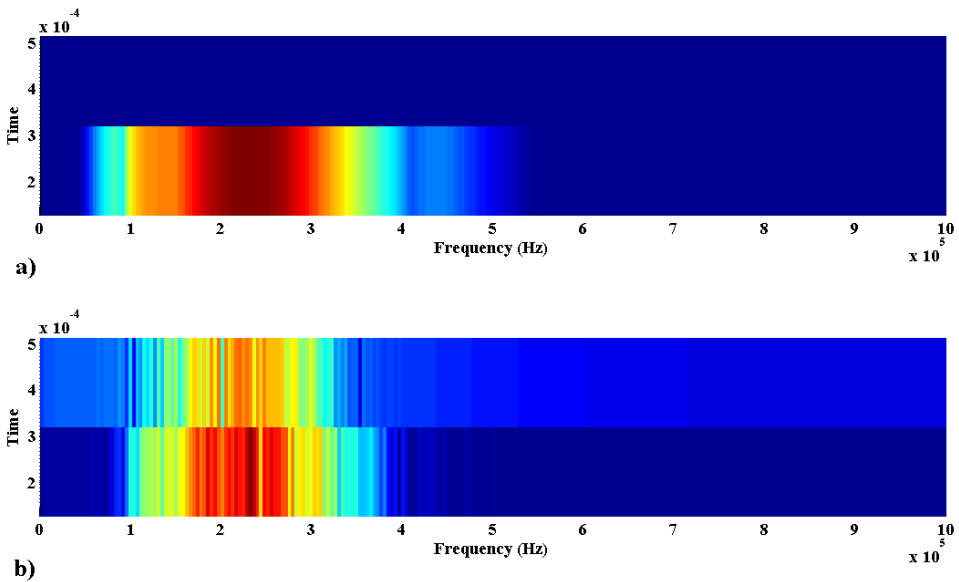


Figure 9: Spectrogram of input and output signal shown in Figure 8a and 8c.

4.1 Damage Index Estimation Using Finite Element Simulated Narrowband Active Sensing

Damage indices based on both the empirical transfer function estimation approach and the correlation analysis approach are evaluated. It is noted that the narrowband sensor signals are collected for the different FE simulated damage conditions discussed earlier. Using empirical transfer function estimation, the respective results for sensor configuration 1 and 2 are shown in Figure 10 and Figure 11. From Figure 10 it can be seen there is a good trend in the damage index only from damage level 6, which is equivalent to 25 mm of crack length. In case of sensor configuration 2 the damage index estimation is more erroneous and can be found that there is no proper trend for the entire damage regime. Also, damage indices based on correlation analysis are evaluated for both sensor configurations 1 and 2. The respective results for sensor configuration 1 and 2 are shown in Figure 12 and Figure 13. Compared to the damage indices estimated using empirical transfer function estimation, the correlation analysis based damage indices show a slightly better trend of cumulative damage growth. It is also seen that, similar to the empirical transfer function estimation approach, the correlation approach shows a better trend for sensor configuration 1 compared to sensor configuration 2. The poor performance of sensor configuration 2 is due to the development of a shadow region that is formed by the propagating cracks in front of the actuator. This leads to a poor damage signature in measurements from sensor configuration 2. On the other hand, the sensor configuration 1 receives the reflected actuator signal from a propagating crack throughout the failure envelope.

Furthermore, it is seen that, the narrowband input based ETFE and CRA approaches show poor performance of damage index estimation during smaller damage growth regime (i.e. below damage level 6 equivalently to 25mm crack length). It must be noted that unlike real life scenario, signals based on FE simulation are noise free. Although the present narrowband based FE simulation signals are noise free, the damage index estimation using these signals fails to provide a clear trend of damage index growth throughout the fatigue life. A potential reason for the lack of trend in the damage index estimation is the narrowband signals central frequency, which may not necessarily be optimal for the chosen actuator and sensor location. Moreover, other structural modes (other than the structural mode associated with the central frequency of the narrowband signal) associated with the local damage are not persistently excited. This leads to a weaker signature in sensor signals. The above mentioned limitations in narrowband based SHM leads to a need for exploring the usefulness of broadband active sensing, which is discussed in the following section.

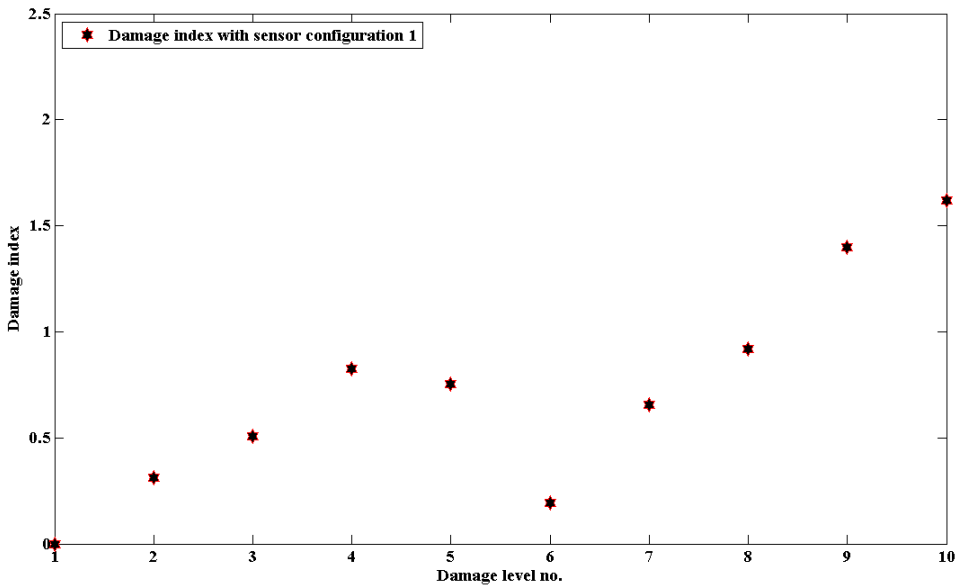


Figure 10: Estimated damage index using ETFE approach and narrowband input signal from sensor configuration 1.

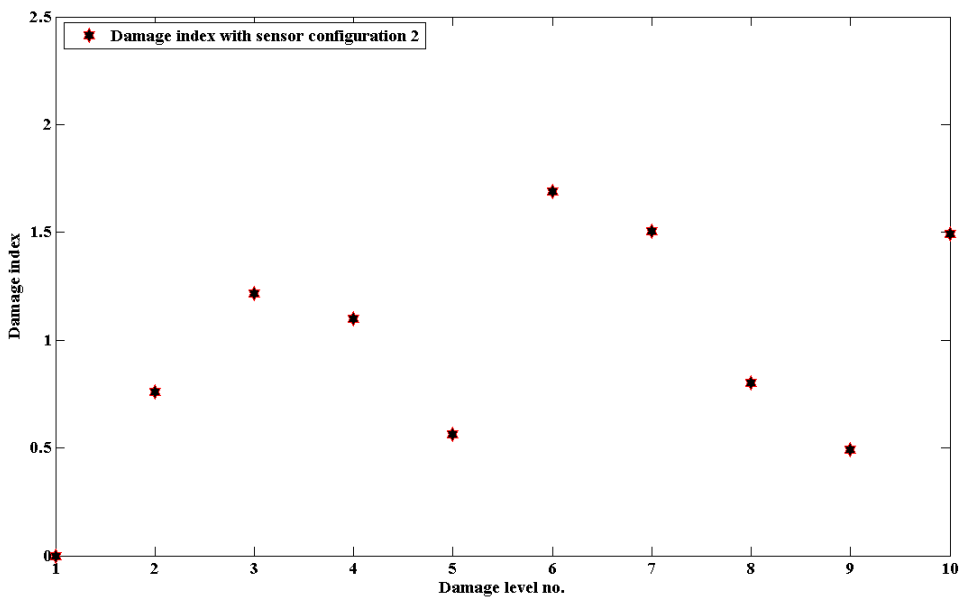


Figure 11: Estimated damage index using ETFE approach and narrowband input signal from sensor configuration 2.

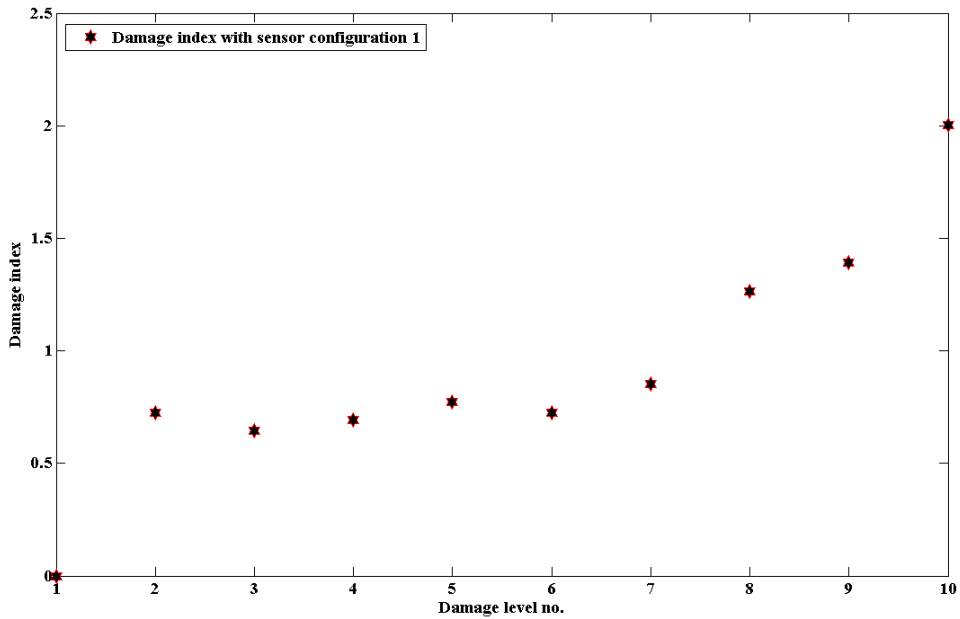


Figure 12: Estimated damage index using correlation analysis approach and narrowband input signal from sensor configuration 1.

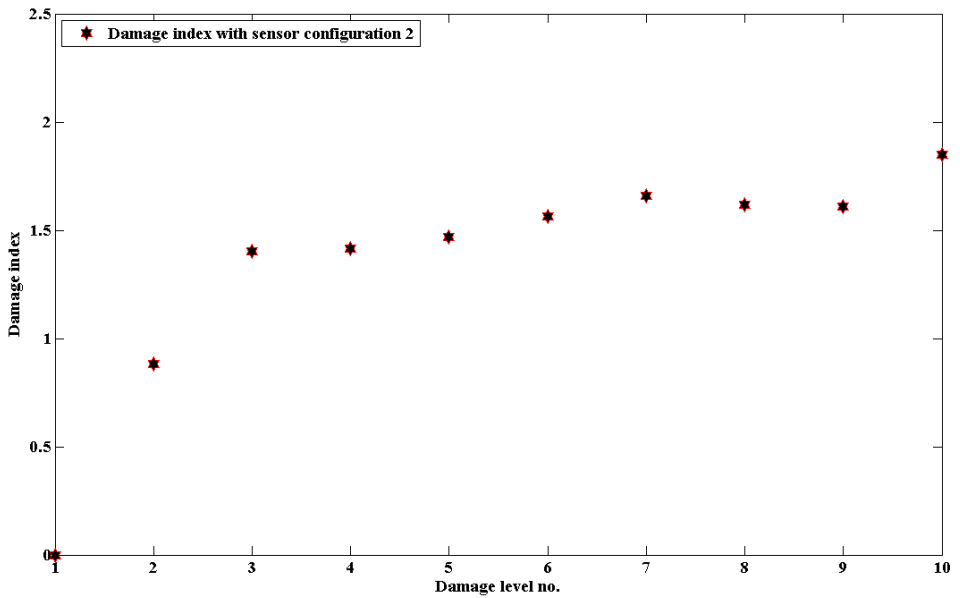


Figure 13: Estimated damage index using correlation analysis approach and narrowband input signal from sensor configuration 2.

4.2 Damage Index Estimation Using Experimental Broadband Active Sensing

Unlike the case of narrowband input, for broadband input it is not required to tune its central frequency with the resonant frequency of the interrogated structure. Also, the tuned central frequency for narrowband input does not necessarily remain optimal as damage progresses. On the contrary, the broadband input consists of multiple sinusoids with different frequencies spreading over a larger envelope that may be affected by damage. It is noted that multiple structural modes are affected by the damage and it is expected that a broadband input will excite those individual structural modes. Hence a broadband input does not require any frequency tuning of the input signal with the resonant frequency of the structure. Using the broadband chirp signals, the damage indices are estimated using Eq. 10 of the ETFE approach and Eq. 11 of the CRA approach. For both sensor configurations the time series damage indices are estimated using the ETFE approach and shown in Figure 14 and Figure 15. Whereas, for the CRA approach, the damage indices estimated using sensor configuration 1 and 2 are shown in Figure 16 and Figure 18. For each set of sensor signals, five different damage indices are estimated. Figure 14 to Figure 18 show the mean damage index and associated 2σ error bounds at different damage levels. For ETFE approach it is found that (refer Figure 14 and Figure 15) up to approximately 82 kcycles, there is a good correlation of cumulative damage growth between estimated damage index and available visual measurements (as shown in Figure 4) for both sensor configurations 1 and 2. However, after 82 kcycles it can be seen that (refer Figure 15) the damage index time series estimated using sensor configuration 2 does not show an increasing trend. This is due to the creation of a blind zone that leads to weaker signals being received by the sensors in configuration 2. On the other hand, for the entire fatigue loading regime, configuration 1 shows an increasing trend of damage index time series, which is evident in Figure 14. The increasing trend for sensor configuration 1 better resembles the physical phenomenon associated with cumulative damage growth.

In the case of CRA based approach it is found that (ref. Figure 16 and Figure 18) up to approximately 110 kcycles there is a continuous increasing trend of damage index time-series for both sensor configurations 1 and 2. However after 110 kcycles it can be seen that the damage index time-series estimated using sensor configuration 2 (refer Figure 18) does not show an continuous increasing trend. This is again due to the creation of a blind zone that leads to weaker signals being received by the sensors in configuration 2. On the other hand, for the entire fatigue loading regime, configuration 1 shows (refer Figure 16) an increasing trend of damage index time-series. This is more evident when Figure 16 is magnified as seen in Figure 17. It must be noted that although both approaches use the same sensor signals, in both sensor configurations the CRA based approach shows better trend in damage index

growth compared to the ETFE based approach. For example, for sensor configuration 2, the ETFE based approach shows the cumulative damage index growth trend up to 82 kcycles (refer Figure 15), whereas for CRA approach the corresponding trend is up to 110 kcycles (refer Figure 18). As mentioned before, the higher accuracy of the damage index estimated using CRA approach is due to the direct use of cross-covariance coefficients $C_{uy}(m)$ and auto covariance coefficients $C_{uu}(m)$ (refer Eq. 12) rather than performing Fourier transformation of those (refer Eq. 6 and Eq. 7), while evaluating the damage index using ETFE based approach.

In addition to the above mentioned observations Figure 14 to Figure 18 clearly indicate that the rate of damage index growth is higher between 10 to 19 kcycles compared to that after 10 kcycles. This trend is observed for both sensor configuration 1 and 2 and with both damage index estimation approaches. The higher growth rate is possibly due to creation of multiple surface cracks in front of the EDM notch (refer Figure 3). These surface cracks coalesce before forming a visible through crack at 19 kcycles. As seen from Figure 4 these surface cracks were not captured in the image either because the cracks were developed in the opposite side of the specimen (opposite to the camera) or due to lack of clarity in the captured image. For CRA based approach, similar trend in high damage index growth rate is also observed from 140.5 kcycles to 142 kcycles. From Figure 16 and 18 it can be seen at 140.5 kcycles, when the top crack has not initiated (see Figure 4 and 19a), the corresponding damage index was approximately 1.419 for sensor configuration 1 and 1.128 for sensor configuration 2. It can be seen that, at 142 kcycles there is a sudden jump in damage index from 1.419 to 1.973 for sensor configuration 1 and from 1.128 to 1.23 for sensor configuration 2. From the acquired image shown in Figure 19b it is seen that there was no through crack at the top edge of the central hole. The jump in damage index again is possibly due to the development of multiple surface cracks. The snap-shot of the surface cracks coalesces (before the onset of a through crack at the top edge of the central hole) can be clearly seen from Figure 18c. Due to the development of multiple surface cracks, the signals received at the sensors are highly distorted and a jump or high growth in damage index is observed. It is noted that from 140.5 kcycles to 142 kcycles this trend of high damage index growth rate is not observed (refer Figure 14 and 15) for ETFE based approach. This is because the ETFE based approach is not sensitive as CRA approach to distinguish between large crack opening and the corresponding precursory surface crack around it. In addition to the above mentioned drawbacks in ETFE approach, it is also seen that the 2σ error bounds for correlation approach (refer Figure 16 and Figure 18) is significantly narrower compared to the ETFE based 2σ error bounds (refer Figure 14 and Figure 15). The lower 2σ error bounds in case of CRA approach compared to ETFE approach is due to the direct use of

time response signals rather than Fourier transformed correlation coefficients used in ETFE approach.

4.3 Noise Sensitivity Evaluation

In addition to the damage index estimation at different damage levels, the sensitivity of the damage index to noise is evaluated by estimating the index from 500 different sets of observations acquired at a particular damage level (in this case at the healthy condition). The 500 observation sets are collected at 2 second intervals by repeatedly exciting the actuator. The corresponding damage indices for ETFE based approach are plotted in Figure 20. For the ETFE approach, it can be seen that, the value of each damage index is restricted to 0.5 for all 500 sets of observations. This observation suggests that damage indices greater than 0.5 not only have the contribution from measurement noise but also have the contribution from the change in damage state. This sensitivity analysis also suggests that at a particular damage level, the maximum variation (due to electrical noise) of estimated damage index is limited to 0.5. The sensitivity information can also be correlated with the 2σ error bound presented in Figure 14 and Figure 15, which shows that the maximum variation in damage index about its mean damage level does not exceed 0.5. Similar sensitivity analysis is also performed for the CRA approach. The corresponding damage indices for 500 different sets of observations are estimated and are presented in Figure 21. It can be seen that the damage index value in this case is much smaller than the one, obtained for the ETFE based approach. The damage index is restricted to a value of 0.1, except for few outliers, for all 500 sets of observations. The above sensitivity analysis can also be correlated with the 2σ error bound, shown in Figure 16 and Figure 18, which shows that the maximum variation in the damage index (due to electrical noise) at any particular damage level is not more than 0.1. Comparison of the error bound and the sensitivity analysis results also shows that the CRA approach is less sensitive to noise compared to the ETFE based approach.

5 Conclusion

The use of two nonparametric system identification techniques empirical transfer function estimation approach and correlation analysis approach was investigated to estimate the time-series fatigue damage states. Novel dual sensing method is used to perform ultrasound input based system identification. From the numerical study it was found that the correlation based damage index estimation follows a better trend of cumulative damage growth compared to the empirical transfer function estimation based approach. The damage indices were estimated using both narrowband based burst input and broadband based chirp input. It was found that

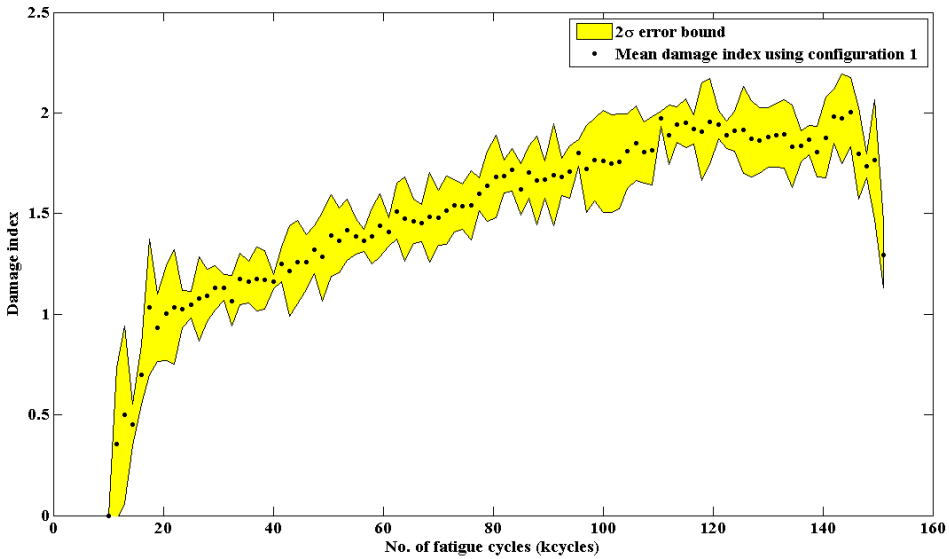


Figure 14: Time series damage index estimated using ETFE approach and sensor configuration 1

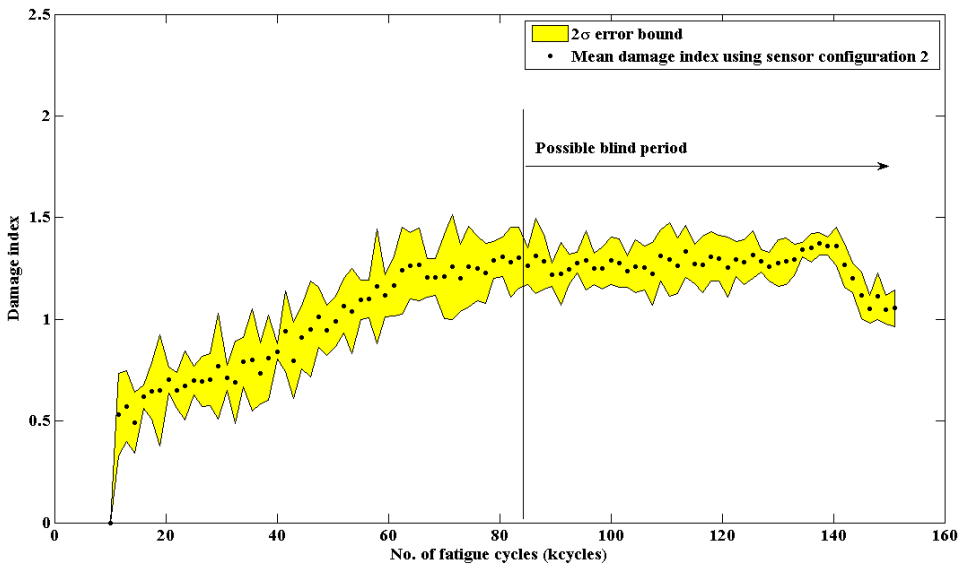


Figure 15: Time series damage index estimated using ETFE approach and sensor configuration 2

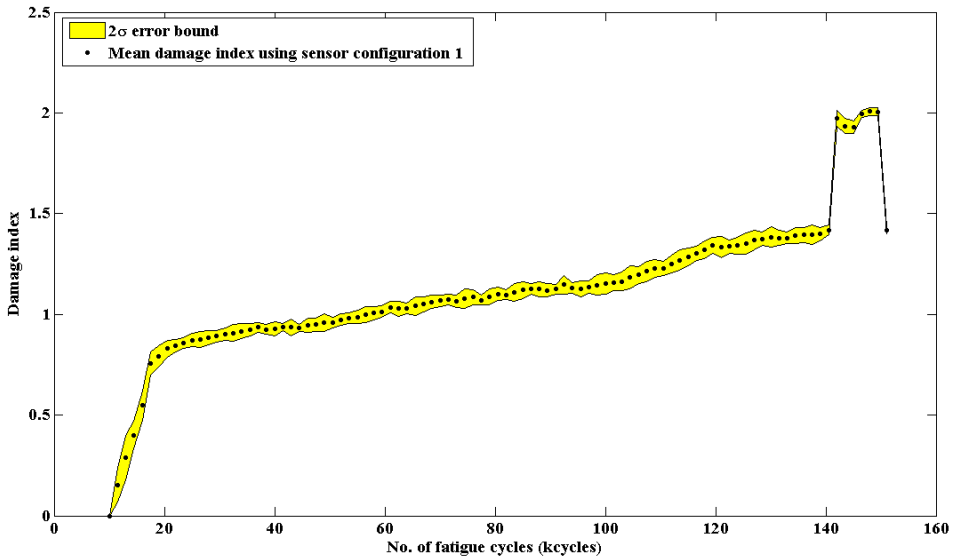


Figure 16: Time series damage index estimated using correlation analysis approach and sensor configuration 1

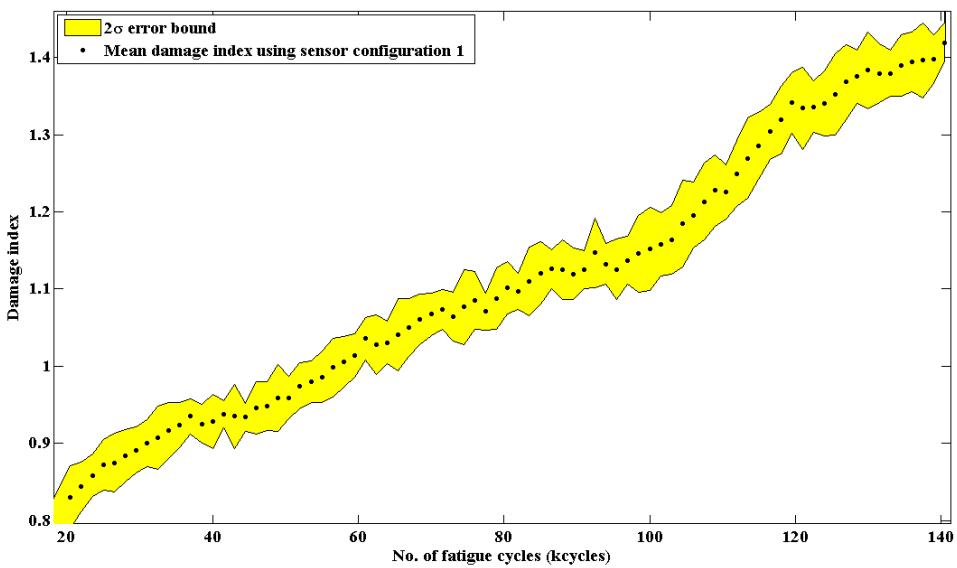


Figure 17: Magnified (from 20 cycles to 140 cycles) version of Figure 16

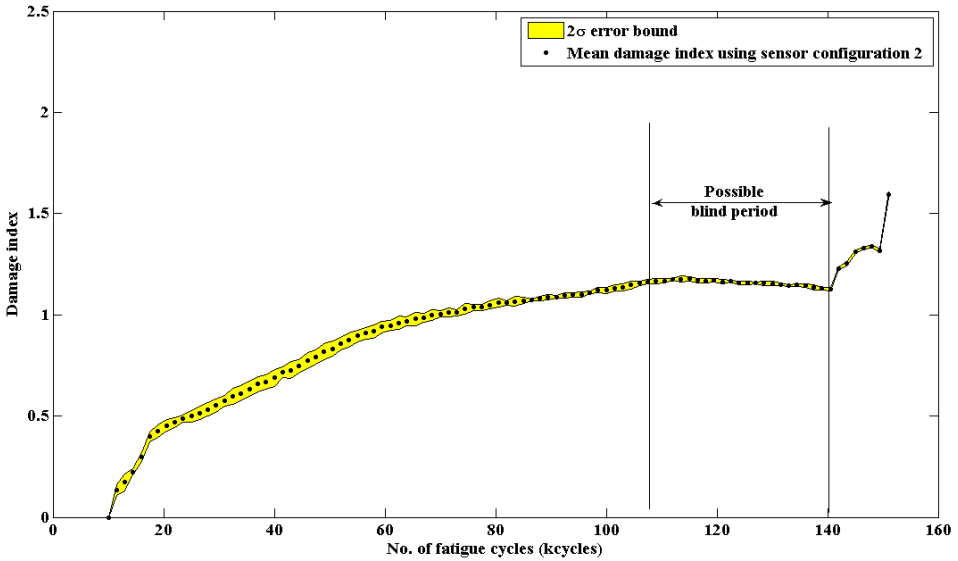


Figure 18: Time series damage index estimated using correlation analysis approach and sensor configuration 2

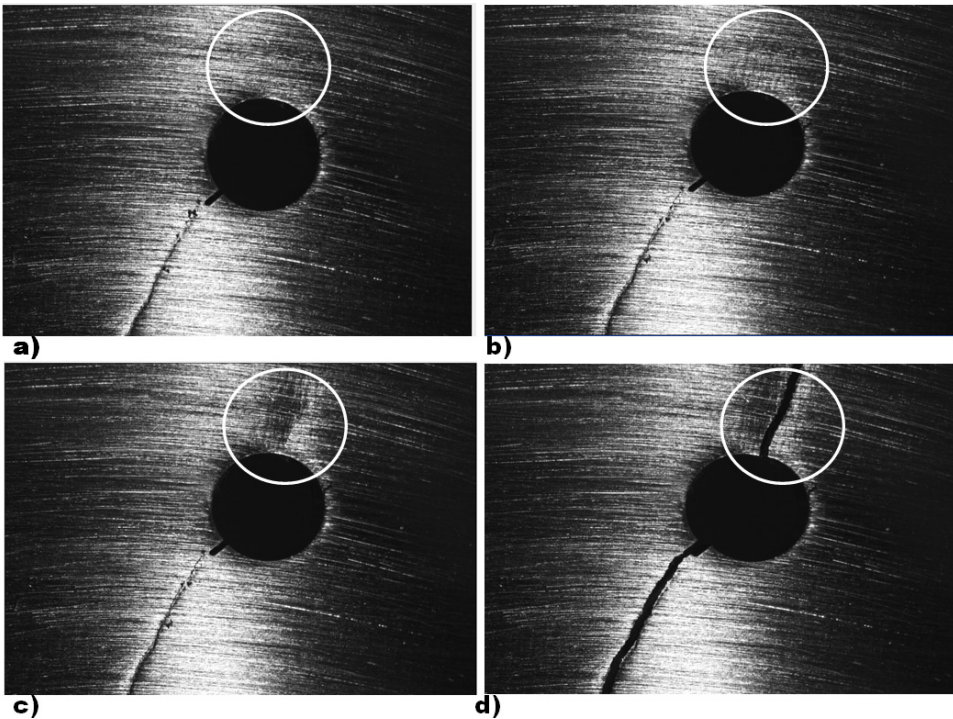


Figure 19: Visual image snapshots at a) 140.5 kcycles b) 142 kcycles c) 149.5 kcycles d) 151 kcycles.

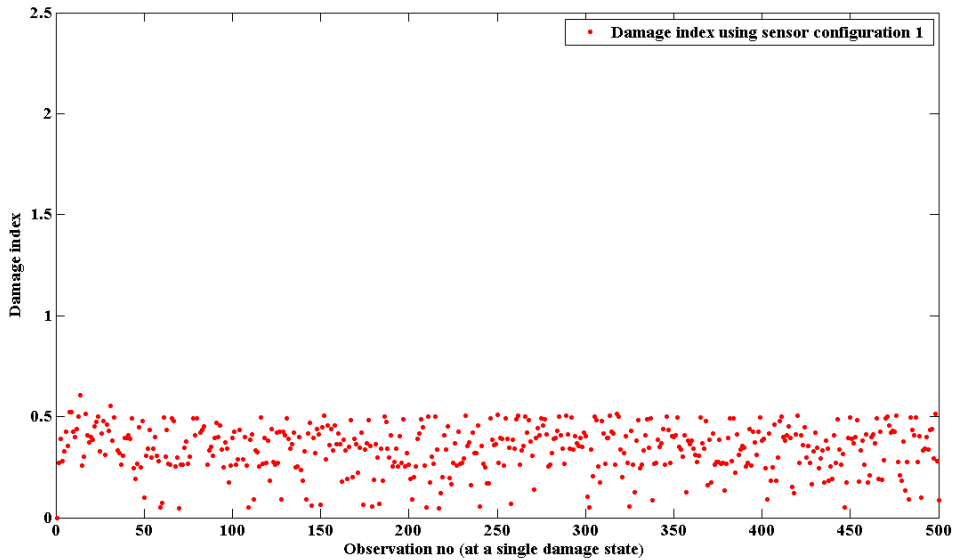


Figure 20: Check of the sensitivity of the damage index estimation using ETFE approach and 500 different sets of observation collected at a particular damage level.

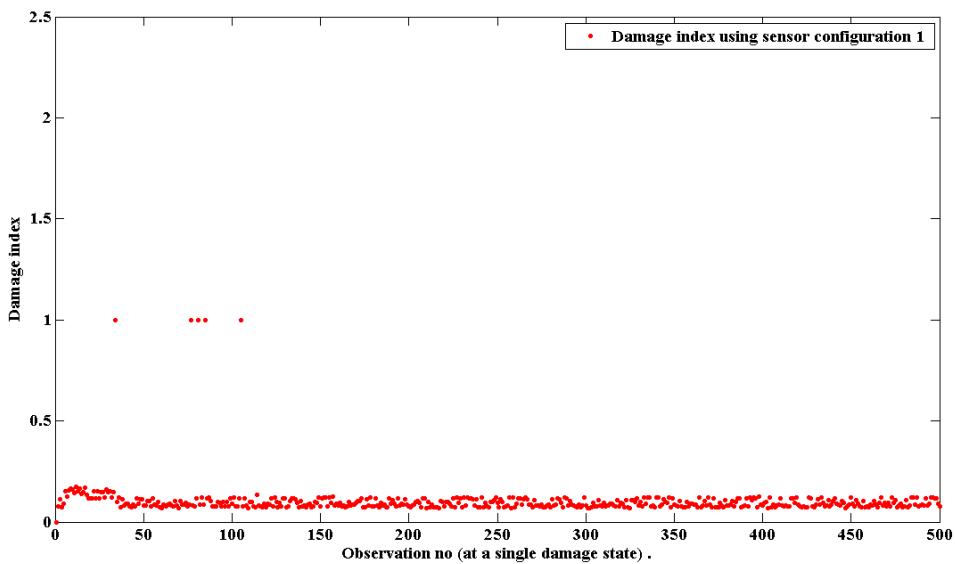


Figure 21: Check of the sensitivity of the damage index estimation using CRA and 500 different sets of observation collected at a particular damage level.

the damage index estimation based on the broadband chirp input outperforms the narrowband input based damage index estimation. In addition, two different sensor configurations were studied. It was observed that the sensor configuration with sensors near the actuator was more effective for time series damage state estimation than the sensor configuration that had sensors placed away from the actuator. The time-series damage estimation approaches are validated on a complex Al-2024 cruciform specimen undergoing biaxial cyclic loading. The proposed unsupervised approaches can be useful for on-line health monitoring of any complex structure.

Acknowledgement: This research was supported by the MURI Program, Air Force Office of Scientific Research, and grant number: FA9550-06-1-0309; Technical Monitor, Dr. David S Stargel.

References

Farrar, C. R.; Sohn, H.; et. al. (2003): Damage Prognosis: Current Status and Future Needs. Technical Report LA-14051-MS, Los Alamos National Laboratory, Los Alamos National Laboratory, USA, 2003.

Farrar, C. R.; Worden, K.; et. al. (2007): Nonlinear System Identification for Damage Detection. Technical Report LA-14353, Los Alamos National Laboratory, Los Alamos National Laboratory, USA, 2007.

Giurgiutiu, V.; Cuc, A. (2005): Embedded non-destructive evaluation for structural health monitoring, damage detection, and failure prediction. *Shock Vib. Digest*, vol. 37, pp. 83–105.

Giurgiutiu, V.; Cuc, A. (2008): Current Issues in Vibration-Based Fault Diagnostics and Prognostics. *Proceedings of the SPIE's 9th Annual International Symposium on Smart Structures and Materials and 7th Annual International Symposium on NDE for Health Monitoring and Diagnostics, March 17-21, San Diego, CA, USA.*

Iyyer, N.; Sarkar, S.; Merrill, S.; Phan, N. (2007): Aircraft life management using crack initiation and crack growth models - p-3c aircraft experience. *Int. J. of Fatigue*, vol. 29, pp. 1584–1607.

Klein, V.; Morelli, E. (2006): *Aircraft System Identification: Theory and Practice*. AIAA Education Series, AIAA, USA.

Ljung, L. (1999): *System Identification: Theory for the User*. Prentice-Hall, Cambridge, MA.

Mohanty, S.; Chattopadhyay, A.; Peralta, P. (2009): Adaptive Residual Useful Life Estimation of a Structural Hotspot. *Journal of Intelligent Material Systems and Structures*.

Mohanty, S.; Chattopadhyay, A.; Wei, J.; Peralta, P. (2009): Real time Damage State Estimation and Condition Based Residual Useful Life Estimation of a Metallic Specimen under Biaxial Loading. *Structural Durability and Health Monitoring Journal*, vol. 5, pp. 33–55.

Park, G.; Rutherford, C. A.; et. all (2005): High-Frequency Response Functions for Composite Plate Monitoring with Ultrasonic Validation. *AIAA Journal*, vol. 43, pp. 2431–2437.

Park, S.; Yun, C. B.; Roh, Y.; Lee, J. (2006): PZT-based active damage detection techniques for steel bridge components. *Smart Materials and Structures*, vol. 15, pp. 957–966.

Rivera, D.; Lee, H.; Mittelmann, H.; Barun, M. (2007): High-Purity Distillation - Using plant-friendly multisine signals to identify a strongly interactive process. *IEEE Control Systems Magazine*, vol. 27, pp. 72–89.

Xiang-Gen, X. (1997): System identification using chirp signals and time-variant filters in the joint time-frequency domain. *IEEE Transactions on Signal Processing*, vol. 45, pp. 2072 – 2084.